Performance Enhancement in Dye-Sensitized Solar Cells with Composite Mixtures of TiO$_2$ Nanoparticles and TiO$_2$ Nanotubes

D. Maheswari · P. Venkatachalam

Abstract In the present investigation, a new composite nanostructured photoanodes were prepared using TiO$_2$ nanotubes (TNTs) with TiO$_2$ nanoparticles (TNPs). TNPs were synthesized by sol–gel method, and TNTs were prepared through alkali hydrothermal method. Dye-sensitized solar cells (DSSCs) were fabricated with different photoanodes comprising of various ratios of TNTs + TNPs, synthetic indigo dye as photosensitizer, PMII (1-propyl-3-methylimidazolium iodide) as ionic liquid electrolyte and cobalt sulfide as counter electrode. The structures and morphologies of TNPs and TNTs were analyzed through X-ray diffractometer, transmission electron microscope and scanning electron microscopes. The results of the investigation showed that the DSSC-4 made with composite photoanode structure (TNTs/TNPs) (90% of TNPs + 10% of TNTs) had improved photocurrent efficiency (2.11%) than pure TNPs (1.00%) and TNT film (0.78%). Electrochemical impedance spectra revealed that the composite TNTs/TNPs film-based DSSCs possessed the lowest charge-transfer resistances and longest electron lifetime. Hence, it could be concluded that the composite TNTs/TNPs photoanode facilitates the charge transport rate and enhances the efficiencies of DSSCs.

KEY WORDS: TNPs/TNTs composite mixtures; Charge recombination; Electron transport; Photovoltaic parameters; EIS analysis

1 Introduction

Dye-sensitized solar cell (DSSC) has attracted great interest in academic research and in industrial applications owing to their high conversion efficiency and potentially low cost compared to traditional silicon solar cell [1–4]. There are many semiconducting metal oxides such as

D. Maheswari (✉)
Department of Physics, Bharathiar University, Coimbatore 641046, Tamil Nadu, India
e-mail: mahaneerkannan@gmail.com; mahaneerkannan@hotmail.com

P. Venkatachalam
Department of Physics (DDE), Annamalai University, Annamalainagar, Chidambaram 608 002, Tamil Nadu, India

SnO$_2$, ZnO, CeO$_2$ and TiO$_2$; among these, TiO$_2$ is widely used in solar cells, because of the faster electron injection rate compared to other metal oxides [5]. Intense research has been undertaken on the textural properties of nanocrystalline TiO$_2$ film, since they play a key role in light-harvesting solar cells [6–8]. Photoanode is the most important part of DSSC; many investigations are carried out with great enthusiasm and with more excellent structure to improve the efficiency of DSSC [9, 10]. The key parameter that determines the efficiency of light harvesting in DSSC is the surface area of TiO$_2$ material and charge carrier transport in semiconductor electrode. Due to recombination in TiO$_2$ semiconductor electrode, the collection of photoinjected electrons compete with recombination, so a high charge collection efficiency is required and that must be faster than recombination rate. In this sense, crystalline nanotubes (NTs)- and nanowires (NWs)-based photoelectrodes have been investigated to improve

electron collection efficiencies [11–13]. The reported efficiency of pure TNTs DSSCs is 2.61%, which is much lower than that of pure TNPs DSSCs of 5.2% [14, 15]. The main reason is the internal surface area of TNT-based photoanode is much smaller than that of TNP-based photoanode resulting in lower dye absorption and lower photon absorption. But mesoporous TNPs can provide a large surface area for dye loading, but electron loss is huge, whereas TNTs provide higher electron transport capability and stronger light scattering propagation [16, 17]. Therefore, the composite film of TNTs and TNPs could be applied in the fabrication of photoelectrode, which is expected to increase the electron collection efficiency, the amount of dye loading, as well as to reduce the electron recombination rate [18–20]. Ohsaki et al. [21] reported the electron lifetime of TNTs is three times larger than TNPs resulting in improvement of diffusion length. Kuang et al. [22] showed template-assisted TNTs enrolled 2.7% efficiency and TNPs/TNTs enrolled 3.2% efficiency.

In DSSCs, the sensitizing dye is one of the key components for high-power conversion efficiency and the Ru (II) complex is the most efficient heterogeneous charge-transfer sensitizer that is widely used in the nanocrystalline TiO_2-based DSSCs [23]. However, the main drawback of the Ru (II) complex sensitizer is expensive and requires careful synthesis and tricky purification steps. The use of natural pigments as sensitizing dyes for the conversion of solar energy into electricity represents a very attractive alternative, due to significant benefits such as low cost, easy processing, environmental friendliness and low human toxicity. The sensitizing dye should be cheaper, more environmentally friendly than metal-complex dyes and must have narrow absorption spectra. In addition, for efficient regeneration of dye, the oxidized state of dye must be more positive potential than that of the redox electrolyte [24]. Moreover, the photosensitizer species should not form aggregates, should be stable chemically, thermally and must be photostable [25]. Abdullah et al. [26] reported that the absorption spectrum of indigo lies near-infrared region and visible region, which can be observed as a wide band of spectrum. In this work, we prepared an indigo dye, which is an organic compound with a distinctive blue color. Historically, indigo is a natural dye extracted from plants and this process was economically important because blue dyes were once rare [27]. The maximum absorption wavelength is 602 nm.

The use of ionic liquid electrolyte is advantageous due to the high degree of wetting obtained on the fused nanoporous metal oxide electrode as well as its high ionic conductivity. Several imidazolium iodide compounds have been utilized as electrolytes in DSSCs, and impressive photoconversion efficiency was reported [28]. For long-term operation of DSSCs, the usage of liquid electrolytes

containing organic solvents is sensitive to negative stability effects, caused by evaporation or decomposition. Desirable features such as a high electrical conductivity, non-volatility, good ionic mobility and electrochemical stability make them preferable to organic solvent-based electrolytes [29, 30]. Wang et al. [31, 32] reported that the efficiencies of 7% with pure ionic liquid electrolytes and an improved efficiency of 6.6% with binary ionic liquid electrolytes.

In the present investigation, TNPs and TNTs were synthesized by sol–gel method and hydrothermal technique, respectively. Six different working photoanodes were prepared using five pastes of TNTs concentrations of 0, 10, 50, 90 and 100 wt% with TNPs by doctor bladding method and labeled as (DSSC-2 to DSSC-6). Bulk TiO_2 photoanode is used for comparison and labeled as DSSC-1. Dye-sensitized solar cells (DSSCs) were fabricated using synthetic indigo dye as sensitizer with ionic liquid electrolyte PMII (1-propyl-3-methylimidazolium iodide) and cobalt sulfide as counter electrode which is far less expensive, more efficient, more stable and easier to produce in the laboratory [33, 34]. The photovoltaic performance and charge transport properties of various DSSCs were studied.

2 Experimental

2.1 Materials

All chemicals used in this study are of high purity, purchased from Sigma-Aldrich, India, and were used without further purification unless or otherwise stated.

2.2 Preparation of TiO_2 NPs Through Sol–gel Process

TNPs were synthesized using titanium (IV) isopropoxide [TTIP], nitric acid, ethyl alcohol and distilled water. The TTIP was mixed with ethanol, and distilled water was added drop by drop under vigorous stirring for 1 h. This solution was then peptized using nitric acid and heated under reflux at 80 °C for 8 h. After this period, a TiO_2 sol was prepared. The prepared solution was dried and calcined at 450 °C for 1 h in a furnace. TiO_2 nanoparticles were obtained [35].

2.3 Preparation of TiO_2 NTs Through Hydrothermal Process

TNTs were prepared through the hydrothermal process. Two grams of TNPs as prepared by the sol–gel method was mixed with 100 mL of a 10 mol/L NaOH aqueous solution, followed by hydrothermal treatment at 150 °C in a Teflon-lined autoclave for 12 h. After the hydrothermal reaction,

the treated sample was washed thoroughly with distilled water and 0.1 mol/L HCl and subsequently filtered and dried at 80 °C for 1 day. The sample was calcined at 450 °C for 1 h, and TNT is obtained [20, 36].

2.4 Fabrication of Dye-Sensitized Solar Cells

The TiO$_2$ pastes with various ratios of TNPs/TNTs were prepared by mixing ultrasonically for 2 h. The indium tin oxide-coated glass plate (ITO) was cleaned ultrasonically in deionised water and acetone for 10 min. The as-prepared pastes were deposited by doctor blade technique on ITO glass plate with an active area of 1 cm^2. Six different photoanodes were prepared, one with 0% TNTs, second with 100% of TNTs, third with 10% of TNTs, fourth with 50% of TNTs and fifth with 90% of TNTs and TNPs which were, respectively, labeled as DSSC-2, DSSC-3, DSSC-4, DSSC-5 and DSSC-6. One more DSSC was fabricated using bulk TiO$_2$ particles and represented as DSSC-1. These photoanodes were then heated at a rate of 15 °C/min and kept at 500 °C for 30 min. After cooling to 80 °C, these photoanodes were immersed overnight in a solution of synthetic indigo dye for 24 h. One drop of iodine-containing electrolyte (0.6 M 1-methyl-3-propylimidazolium iodide (PMII), 0.1 mol/L LiI, 0.05 mol/L I$_2$, 0.5 mol/L tert-butylpyridine in acetonitrile) was dropped onto the surface of the photoanodes. The cobalt sulfide-coated ITO counter electrode clipped on top of the TiO$_2$ photoelectrodes to form a photovoltaic device.

2.5 Characterization of Dye-Sensitized Solar Cells

The photovoltaic properties of the DSSCs were characterized by recording the photocurrent–voltage (I–V) curves under the illumination of A.M. 1.5 G (100 mW/cm^2). TNPs and TNTs were characterized by X-ray diffraction (X'Pert PRO-PANalytical X-ray powder diffractometer). Micrographs of the samples were observed by TEM (PHILIPS TECNAI 10) and SEM (VEGA3 SB). Specific surface areas of the TiO$_2$ samples were determined by nitrogen adsorption apparatus (Micromeritics ASAP 2020). PEC-S20 solar cell spectral response system was used to measure incident photon-to-current conversion efficiency (IPCE) of the DSSCs. UV–Visible absorption spectrum of the indigo dye was recorded using a Systronics-104 spectrophotometer. Electron impedance spectra of DSSCs were recorded with potentiostat/galvanostat (Gamry 300). The applied bias voltage and AC amplitude were set at an open-circuit voltage of the DSSCs; 10 mV is set between the ITO/counter electrode and the ITO/TiO$_2$/dye photoanode, respectively, and the frequency range explored was 1 mHz to 10^5 Hz. The impedance spectra were analyzed by an equivalent circuit model, interpreting the characteristics of the DSSCs through Zsimpwin software.

3 Results and Discussion

3.1 XRD, SEM and TEM Analysis

The structures and morphologies of TNPs and TNTs were characterized by X-ray diffractometer (XRD), transmission electron microscope (TEM) and scanning electron microscope (SEM). Figure 1 shows the XRD patterns of TNPs and TNTs after annealing at 450 °C. The peaks (101), (004), (200), (105) and (211) are typical peaks of anatase TNPs. From this figure, it could be noticed that the TNPs and TNTs exhibit highly crystallized anatase structure. Figure 2a shows the TEM image of the TNPs, grown at 450 °C having uniform spherical structure and with mean diameter of ∼20 nm. Figure 2b shows the TEM image of TNTs with tube-like uniform structure with an outer diameter of ∼10 nm, inner diameter of 4–6 nm and the length of 50–100 nm. Figure 3 shows the SEM image of TNPs and TNT, respectively. The size of the TNP is 20 nm. SEM image of the sample anatase TNTs exhibits a tube-like structure. The length of the TNTs is several nanometers, their diameter is approximately 10 nm, and they are very uniform, quite clean and smooth-surfaced. It can be seen that the starting material exhibits nanoparticle type and the mean diameter is about 20 nm. After hydrothermal synthesis, the particles were completely converted to TiO$_2$ nanotubes. Most of the TNTs are straight and vertical, though occasionally a few non-vertical TNTs can also be observed. The texture of the TNTs is uniform and reasonably dense, though there are ample voids between the tubes. From the SEM, it could be observed that the external tube diameters fall in 8–10 nm, the internal diameters are between 4–6 nm, and the lengths of nanotubes are up to 100 nm. The dye adsorption depends on the surface area of TNTs (surface area of one TNT = $2\pi rh + \pi r^2$, where r is radius and h is height of the TNT). The Brunauer–Emmett–Teller (BET) surface area of the TNTs is 60 m^2/g shown in Fig. 4. This value is much higher than that of TNPs nanoparticles (20 m^2/g).

IPCE spectrum is a plot of a ratio of the number of output electrons (current) and input photons (irradiance) against wavelengths. The maximum incident photon-to-current conversion efficiency (IPCE) based on indigo was 80% for DSSC-4, 60% for DSSC-5, 50% for DSSC-6, 30% for DSSC-2 and 15% for DSSC-3 (Fig. 5) whose absorption is almost equal to the efficiency obtained with the N3 dye system [37]. The IPCE performance of DSSCs based on indigo dye depends remarkably on the LUMO levels of
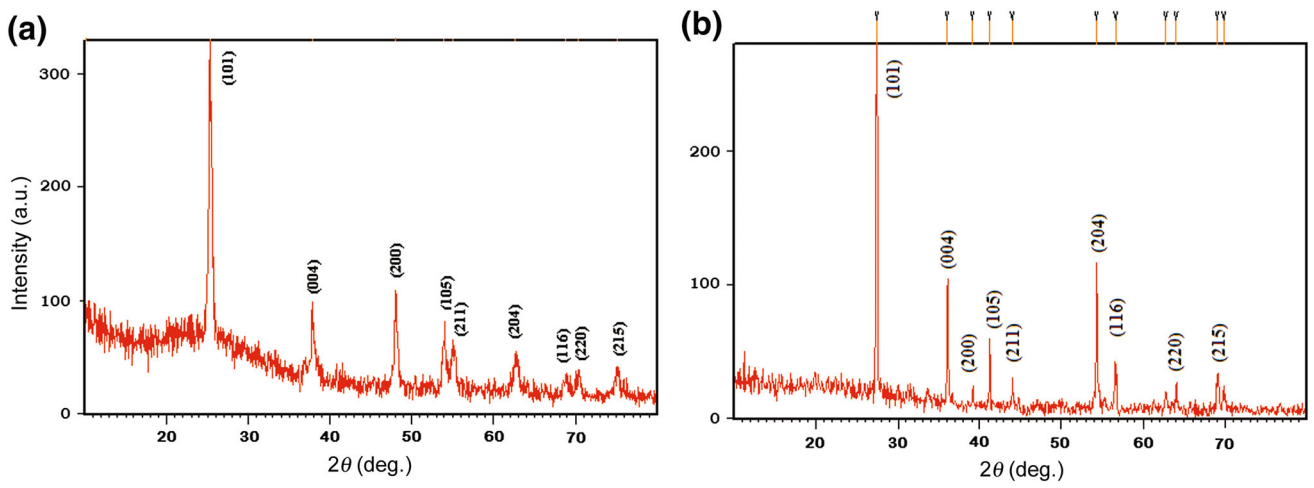
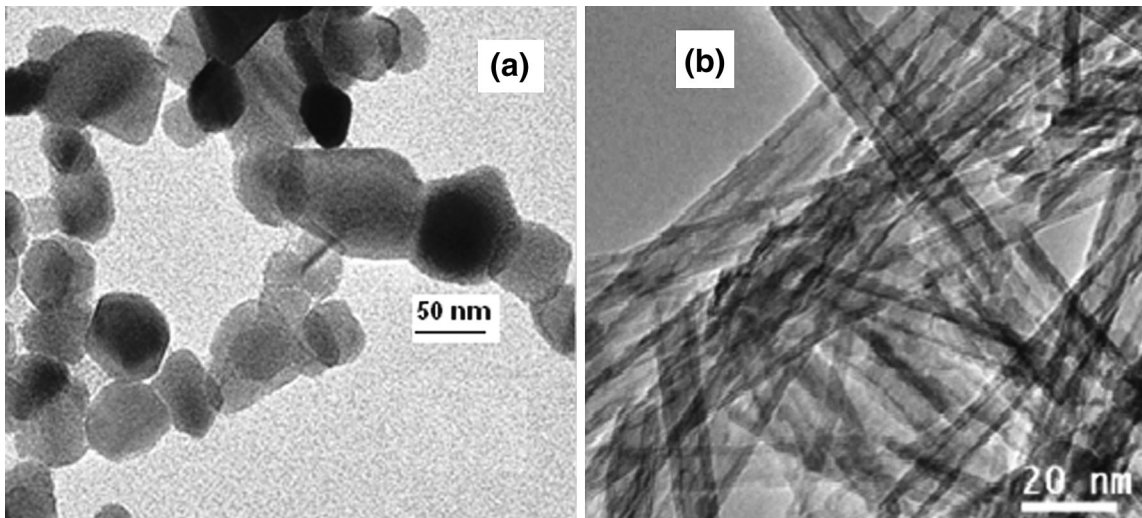**Fig. 1** XRD patterns for TNP **a**, TNT **b** annealed at 450 °C

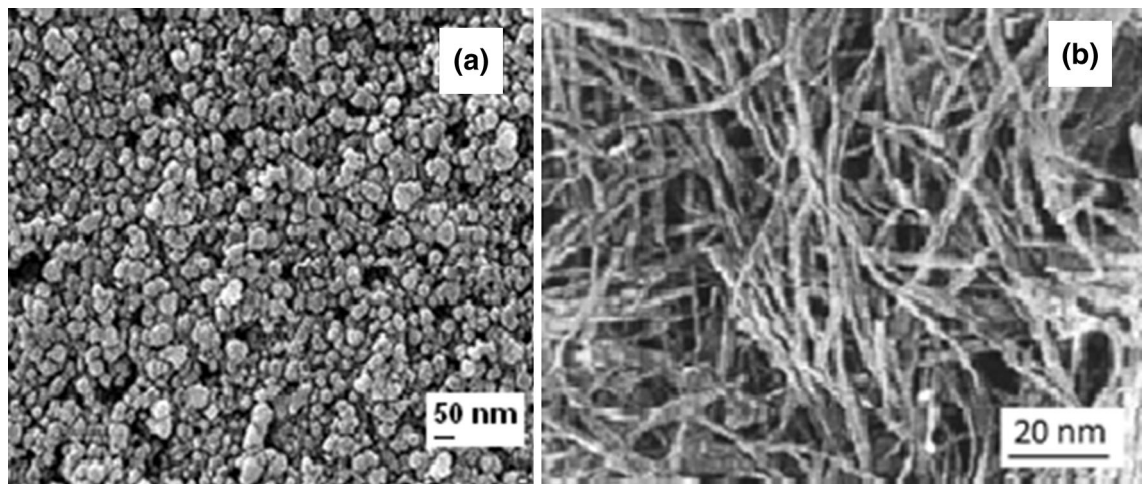**Fig. 2** TEM images for TNP **a**, TNT **b**
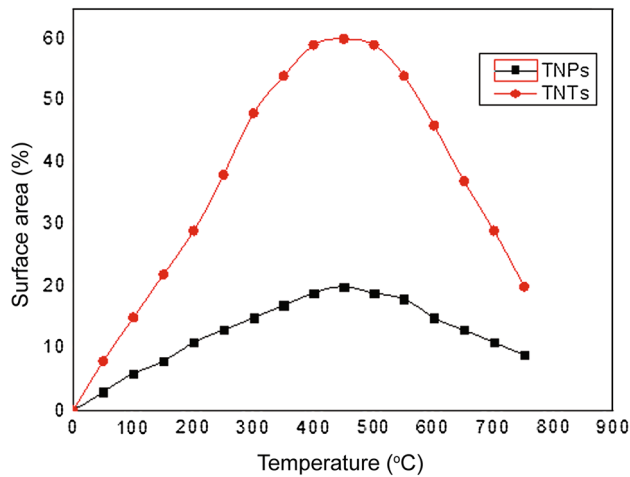

Fig. 3 SEM images for TNPs **a** and TNTs **b**

Fig. 4 Surface area of TNTs and TNPs

Fig. 6 Nyquist plot of DSSCs

Fig. 5 IPCE of photoanodes

Fig. 7 Frequency-phase plot of DSSCs
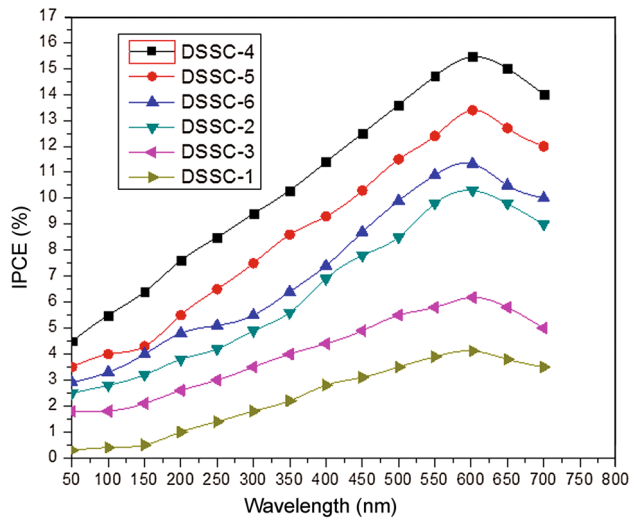
the dyes, which are estimated from the oxidation potential and 0–0 energy of the dye.

3.2 EIS Analysis

Electron transport properties were studied using electrochemical impedance spectroscopy (EIS). Figs. 6 and 7 show the Nyquist and frequency-phase plots of DSSCs, respectively. Figure 6 shows the Nyquist plots corresponding to the DSSCs based on the indigo-sensitized photoanode film under the light intensity of 100 mW/cm². In general, the Nyquist plots exhibit three semicircles, which are attributed to the redox reaction at the cobalt sulfide counter electrode in the high-frequency region, the electron transfer at the TiO₂/dye/electrolyte interface in the middle-frequency region and carrier transport by ions
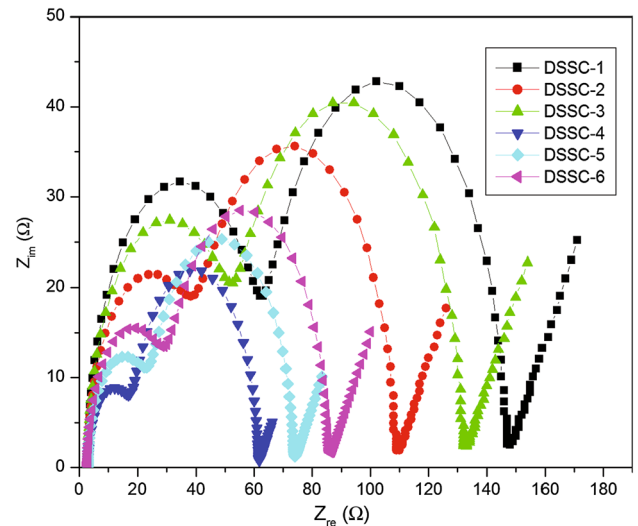
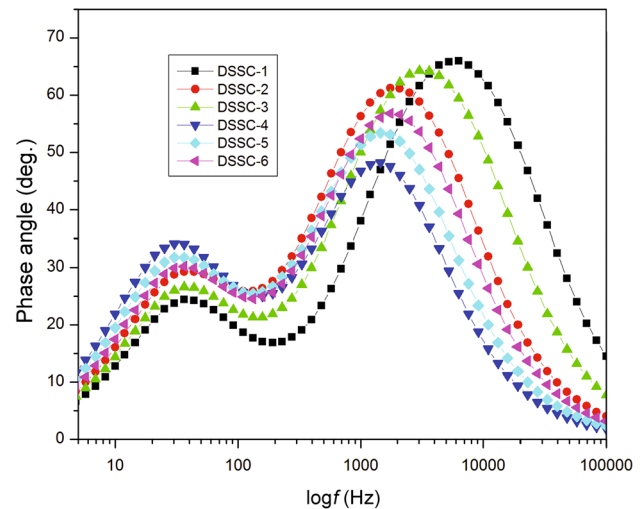within the electrolytes in the low-frequency region [38, 39]. The other useful electrochemical parameters of DSSCs were calculated from the following equations and presented in Table 1.

$$\tau_{\text{eff}} = R_{\text{ct}} C_{\text{ct}}, \tag{1}$$

$$k_{\text{eff}} = \frac{1}{\tau_{\text{eff}}}, \tag{2}$$

$$D_{\text{eff}} = \left(\frac{R_{\text{tr}}}{R_{\text{ct}}}\right)\left(\frac{L_{\text{F}}^2}{\tau_{\text{eff}}}\right), \tag{3}$$

$$L_{\text{n}} = (\tau_{\text{eff}} D_{\text{eff}})^{1/2}, \tag{4}$$

$$\mu = \frac{(D_{\text{eff}} e)}{(K_{\text{B}} T)} = 38.9\, D_{\text{eff}}, \tag{5}$$

Table 1 EIS parameters of DSSCs

DSSCs	R_s (Ω)	R_{rec} (Ω)	R_{ct} (Ω)	C_{rec} (μF)	C_{ct} (μF)	Z_d (Ω-s$^{0.5}$)	k_{eff} (s^{-1})	τ_{rec} (μs)	τ_d (μs)	L_n (μm)	D_{eff} (10^{-5} cm^2/s)	μ (10^{-4} cm^2/V s)	σ (10^{-5} S/cm)	η_{cc} (%)
DSSC-1 (bulk TiO$_2$)	2.996	83.05	60.07	80.67	2.1	2	149	6,699	4,845	11.76	21	80.3	0.075	27
DSSC-2 (100% TNPs)	3	68	37	112	8	1.4	131	7,616	4,144	13.56	24	93.9	0.092	46
DSSC-3 (100% TNTs)	2.996	78.02	50.09	92.66	4.11	1.8	138	7,229	4,641	12.48	22	83.8	0.08	36
DSSC-4 (10% TNPs + 90% TNTs)	2.997	43.09	15.09	230.5	18.1	0.4	100	9,932	3,478	16.89	29	111.18	1.451	65
DSSC-5 (50% TNPs + 50% TNTs)	2.997	49.09	21.12	185.8	14.12	0.8	109	9,120	3,924	15.25	25	99.1	1.273	57
DSSC-6 (90% TNPs + 10% TNTs)	2.997	55.09	27.06	150.7	10.12	1.2	120	8,302	4,077	14.27	22	95.4	1.135	51

$$\sigma = \frac{L_F}{[S(1-P)\,R_{ct}]}, \tag{6}$$

$$\eta_{cc} = 1 - \left(\frac{\tau_d}{\tau_{eff}}\right), \tag{7}$$

$$\text{Conc.} = R_{ct}L_F k_{eff}, \tag{8}$$

where τ_{eff} is effective electron life time, s; k_{eff} is rate of recombination of the electrons in the film, s^{-1}; D_{eff} is effective diffusion coefficient, cm^2/s; L_n is electron diffusion length, μm; μ is electron mobility, cm^2/(V s); σ is electron conductivity, mS/cm; η_{cc} is electron collection efficiency; Conc. is concentration of electrons in the TiO$_2$/dye/electrolyte interface, Ω cm/s; L_F is the film thickness of the photoanode (12 μm), active area of the DSSCs (1 cm^2); P is porosity of the photoanode film (0.6); $\tau_d = R_{ct}C_{rec}$ is electron transport time; e is charge of an electron; K_B is Boltzmann constant; and T is room temperature [40].

From the Nyquist plot, it can be seen that the first and third semicircles are weak when compared to the second semicircle. This largest semicircle represents interfacial charge-transfer resistance R_{rec} of the injected charges to the direct transfer from the photoanode to I$_3^-$ ions at the TiO$_2$/dye/electrolyte interface. From the Fig. 6, the decrease in middle circles is in the order of DSSC-1 > DSSC-3 > DSSC-2 > DSSC-6 > DSSC-5 > DSSC-4, indicating highest charge-transfer resistance at the TiO$_2$/dye/electrolyte interface for DSSC-1. It can be found from Table 1, the R_{rec} value decreases for composite photoanode (90% NP + 10% NT) when compared to pure TNTs and TNPs suggesting high surface area of TNPs/TNTs and more adequate pore size for facile transport of the redox couple in the TNPs interface, thereby reduces corresponding resistance at the interface. The chemical capacitance value C_{rec} and τ_{rec}, L_n, D_{eff}, μ, σ, η_{cc} at the TiO$_2$/dye/electrolyte interface increases for TNTs/TNPs photoanode DSSC [41]. In the composite photoanode, the lower R_{rec} suggests that each nanotubule makes more difficult for an electron to jump outside the nanostructure than to stay within the structure during diffusion; this explains the high collection efficiencies and thus high short-circuits photocurrents. The hole transport to electrolyte via the different channels can prevent the charge recombination at the TiO$_2$/redox electrolyte interface and leads to the electron diffusion, and transport becomes easy. Therefore, the DSSCs based on the composite TNTs/TNPs film have the lower values of R_{rec}, R_{ct} and the longer electron lifetime, and consequently, this leads to an enhanced conversion efficiency of the cell [20]. Figure 7 shows the frequency-phase plots of EIS spectra for the DSSCs, made with different photoelectrodes. Two characteristic peaks, associated with the transfer of the photogenerated electrons at the surface of composite

TNTs/TNPs and the conducting electrodes, are clearly observed. The frequency peak in the high-frequency region can be ascribed to the charge transfer at the interfaces of the electrolyte/counter electrode, and the other low-frequency region to the accumulation/transport of the injected electrons with TNPs/TNTs porous film and the charge transfer at the interfaces of electrolyte, respectively. From the frequency-phase plots in the lower- and higher-frequency regimes, it can be seen that the frequency peak of DSSC-4 (90% NP + 10% NT) is shifted to lower frequency when compared with other DSSCs. The peak shifted to a lower frequency indicates an increased lifetime in PMII-containing electrolytes. The longest lifetime implies a lower recombination rate and enhanced electron collection efficiency. Therefore, the interface charge recombination of TNPs between the photoinjected electron and electrolyte materials is reduced after the TNTs decoration [42].

3.3 Current–Voltage Characteristics

The current–voltage characteristics of various DSSCs are presented in Fig. 8, and the parameters are given in the
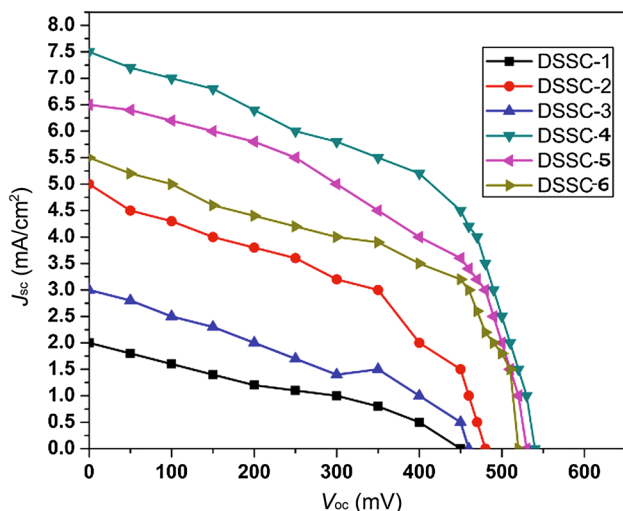
Fig. 8 Current–voltage characteristics of DSSCs

Table 2. From the Table 2, it could be observed that DSSC-4 showed highest efficiency when compared to other DSSCs, the parameters are $V_{oc} = 700$ mV $J_{sc} = 12.8$ mA/cm^2, $V_{max} = 640$ mV, FF = 81.54, $\eta = 2.11\%$, and the improved J_{sc} of the DSSC-4 (90% NP + 10% NT) was attributed to ultrafast and directional electron movement, curtail electron diffusion length, and the light scattering effect. This is because of TNPs/TNTs film has large surface area and more scattering centers, so more dye absorption is obtained. Such a behavior in photocurrent density with TNPs/TNTs film was observed in previous reports as well [43]. TNPs meet the requirement of absorbing dye; it brings about, at the same time, many opportunities for the recombination of photoinjected electrons and the oxidized dye and/or the electron acceptors in the electrolyte. TNTs can enhance the light-harvesting, straight pathway electron transport and also have no serious light loss due to back scattering. Therefore, the design of the (90% TNPs + TNTs 10%) film balances the surface area and the light scattering; thus, the performance of DSSC with TNTs/TNPs electrode is higher than those with pure TNPs or TNTs electrode.

$$FF = \frac{I_m \times V_m}{I_{sc} \times V_{oc}}, \qquad (9)$$

where FF is the fill factor, I_{sc} is short-circuit current, V_{oc} is the open-circuit voltage, I_m is the maximum current, and V_m is the maximum voltage

$$\eta = \frac{V_{oc} \times J_{sc} \times FF}{Pin}. \qquad (10)$$

By incorporation of TNTs (10%) into the TNPs film, the V_{oc} value changes dramatically from 630 to 700 mV as the concentration of TNTs increases. Meanwhile, the J_{sc} and FF values of the cell also increased from 9.1 to 14.8 mA/cm^2 and 69.77 to 81.54 when the TNTs were employed. The FF and efficiency were calculated using Eqs. (9) and (10). The enhancement of the photocurrent efficiency is observed in composite DSSCs—4, 5 and 6 when compared to bare DSSC—1, 2 and 3. It can be attributed to the closely packed structure of TNTs/TNPs in the photoanodes of DSSCs—4, 5 and 6 and loosely packed structure in DSSC—1, 2 and 3, which leads to larger

Table 2 Current–voltage characteristics of various DSSCs

Photoelectrode	V_{oc} (mV)	J_{sc} (mA/cm^2)	V_{max} (mV)	J_{max} (mA/cm^2)	FF (%)	η (%)
DSSC-1 (bulk TiO$_2$)	450	2.0	310	1.0	34	0.30
DSSC-2 (100% TNPs)	480	5.0	335	3.0	42	1.00
DSSC-3 (100% TNTs)	460	3.0	350	1.5	38	0.52
DSSC-4 (90% TNPs + 10% TNTs)	540	7.5	440	4.5	50	2.03
DSSC-5 (50% TNPs + 50% TNTs)	530	6.5	420	4.0	49	1.69
DSSC-6 (10% TNPs + 10% TNTs)	520	5.5	380	3.5	47	1.34

specific surface area of TNTs/TNPs composite when compared to TNPs and TNTs [20].

4 Conclusions

DSSCs were fabricated with TiO_2 working electrode made of different weight ratios of TNTs with TNPs, and the corresponding photocurrent efficiencies and impedance spectra were measured. It is observed that DSSC made with composite mixtures of 90% TNPs + 10% TNTs showed higher efficiency (2.11%) compared to TNPs (~ 1.00%), TNTs (~ 0.78%), (10% TNP + 90% TNT) 1.37% and (50% TNT + 50% TNP) 1.72%. From EIS data, it can be concluded that for the cell containing TNTs, formation of a space charge layer at the surface of the electrode effectively promotes the separation of photogenerated charge carriers and prevents recombination of the electron with the hole carriers. Therefore, the TNPs layer with the 10% of TNTs serves as the active photolayer. In the present investigation, with an optimized ratio of (10% TNTs + 90% TNPs) in the photoelectrode, an enhancement of the maximum energy conversion of ~ 170% has been increased in DSSC-4 when compared to other DSSCs. It is hopeful that the composite structure electrode will play larger potential superiority compared to single structure electrode and can be extended to other composite structure for improving the efficiency of DSSC.

References

[1] B. O'Regan, M. Grätzel, Nature **353**, 737 (1991)
[2] M. Grätzel, J. Photochem. Photobiol. C **4**, 145 (2003)
[3] M. Grätzel, J. Photochem. Photobiol. A **164**, 3 (2004)
[4] A.Y. El-Etre, S.M. Reda, Appl. Surf. Sci. **256**, 6601 (2010)
[5] P. Tiwana, P. Docampo, M.B. Johnston, H.J. Snaith, L.M. Herz, ACS Nano **5**, 5158 (2011)
[6] C.J. Barbe, F. Arendse, P. Comte, M. Jirousek, F. Lenzmann, V. Shklover, J. Am. Ceram. Soc. **80**, 3157 (1997)
[7] Z. Wang, C. Huang, Y. Huang, Y. Hou, P. Xie, B. Zhang, H. Cheng, Chem. Mater. **13**, 678 (2001)
[8] Y.C. Liu, Y.F. Lu, Y.Z. Zeng, C.H. Liao, J.C. Chung, T.Y. Wei, Int. J. Photoenergy (2011). doi:10.1155/2011/619069
[9] M. Law, L.E. Greene, J.C. Johnson, R. Saykally, P.D. Yang, Nat. Mater. **4**, 455 (2005)
[10] A.O.T. Patrocínio, E.B. Paniago, R.M. Paniago, N.Y.M. Iha, J. Phys. Chem. C **114**, 17594 (2010)
[11] M. Rodriguez-Reyes, H.J. Dorantes-Rosales, J. Sol-Gel. Sci. Technol. **59**, 658 (2011)
[12] G.K. Mor, O.K. Varghese, M. Paulose, C.A. Grimes, Adv. Funct. Mater. **15**, 1291 (2005)
[13] K. Zhu, R.N. Nathan, M. Alexander, J.F. Arthur, Nano Lett. **7**, 69 (2007)
[14] G.K. Mor, K. Shankar, M. Paulose, O.K. Varghese, C.A. Grimes, Nano Lett. **6**, 215 (2006)
[15] C.C. Chen, H.W. Chung, C.H. Chen, H.P. Lu, C.M. Lan, S.F. Chen, L.Y. Luo, C.S. Hung, E. Wei, G. Diau, J. Phys. Chem. C **112**, 19151 (2008)
[16] T.H. Meen, W. Water, W.R. Chen, S.M. Chao, L.W. Ji, C.J. Huang, J. Phys. Chem. Solids **70**, 472 (2009)
[17] K. Zhu, T.B. Vinzant, N.R. Neale, A.J. Frank, Nano Lett. **7**, 3739 (2007)
[18] R. Mohammadpour, A. Iraji zad, A. Hagfeldt, G. Boschloo, Phys. Chem. Chem. Phys. **12**, 21487 (2001)
[19] C. Kang, Y. Xie, E. Xie, Optoelectron. Adv. Mater. Rapid Commun. **5**, 518 (2011)
[20] C.H. Lee, S.W. Rhee, H.W. Choi, Nanoscale Res. Lett. **7**, 48 (2012)
[21] Y. Ohsaki, N. Masaki, T. Kitamura, Y. Wada, T. Okamoto, T. Sekino, K. Niihara, S. Yanagida, Phys. Chem. Chem. Phys. **7**, 4157 (2005)
[22] D. Kuang, C. Klein, S. Ito, J.E. Moser, R. Humphry-Baker, S.M. Zakeeruddin, M. Grätzel, Adv. Funct. Mater. **17**, 154 (2007)
[23] R.A. Caruso, M. Antonietti, M. Giersig, H.P. Hentze, J. Jia, Chem. Mater. **13**, 1114 (2001)
[24] S. Hwang, H.H. Lee, C. Park, C.H. Lee, C. Kim, C. Park, M.H. Lee, W. Lee, J. Park, K. Kim, C. Park, N.G. Kim, Chem. Commun. **46**, 4887 (2007)
[25] F. de Angelis, S. Fantacci, A. Selloni, M. Grätzel, M.K. Nazeeruddin, Nano Lett. **7**, 3189 (2007)
[26] M.I. Abdullah, M.R. Saeed, A. Janjua, A. Mahmood, S. Ali, M. Ali, Bull. Korean Chem. Soc. **34**, 2093 (2013)
[27] F. Cervantes-Navarro, D. Glossman-Mitnik, J. Photochem. Photobiol. A Chem. Rev. **255**, 24 (2013)
[28] X.J. Chen, J. Zhao, J.Y. Zhang, L.H. Qiu, D. Xu, H.G. Zhang, X.Y. Han, B.Q. Sun, G.H. Fu, Y. Zhang, F. Yan, J. Mater. Chem. **12**, 18018 (2012)
[29] V. Armel, J.M. Pringle, M. Forsyth, D.R. Mac Farlane, D.L. Officer, P. Wagner, Chem. Commun. **46**, 3146 (2010)
[30] X. Pan, M. Wang, X.Q. Fang, C.N. Zhang, Z.P. Huo, S.Y. Dai, Sci. China Chem. **56**, 1463 (2013)
[31] P. Wang, S.M. Zakeeruddin, I. Exnar, M. Grätzel, Chem. Commun. **8**, 2972 (2002)
[32] P. Wang, S.M. Zakeeruddin, R. Humphry-Baker, M. Grätzel, Chem. Mater. **16**, 2694 (2004)
[33] Z.S. Yang, C.Y. Chen, C.W. Liu, H.T. Chang, Chem. Commun. **46**, 5485 (2010)
[34] J.Y. Lin, J.H. Liao, S.W. Chou, Electrochim. Acta **56**, 8818 (2011)
[35] A. Fujishima, T.N. Rao, D.A. Tryk, J. Photochem. Photobiol. C **29**, 1 (2000)
[36] K. Zhu, N.R. Neale, A. Miedaner, A.J. Frank, Nano Lett. **7**, 69 (2007)
[37] K. Hara, Z.S. Wang, T. Sato, A. Furube, R. Katoh, H. Sugihara, Y. Dan-oh, C. Kasada, A. Shinpo, S. Suga, J. Phys. Chem. B **109**, 15476 (2005)
[38] B. Tan, Y. Wu, J. Phys. Chem. B **110**, 15932 (2006)
[39] B. Tan, Y. Wu, J. Phys. Chem. B **110**, 2087 (2006)
[40] J. Bisquert, J. Phys. Chem. B **106**, 325–333 (2002)
[41] J. Nelson, Coord. Chem. Rev. **248**, 1181 (2004)
[42] J. Van de Lagemaat, N.G. Park, A.J. Frank, J. Phys. Chem. B **104**, 2044 (2008)
[43] G. Schlichthorl, N.G. Park, A.J. Frank, J. Phys. Chem. B **103**, 782 (1999)